Articles

The So-Called *Listeria innocua* Ferritin Is a Dps Protein. Iron Incorporation, Detoxification, and DNA Protection Properties†

Meihong Su,‡ Stefano Cavallo,§ Simonetta Stefanini,§ Emilia Chiancone,§ and N. Dennis Chasteen*,‡

Department of Chemistry, University of New Hampshire, Durham, New Hampshire 03824, and Istituto di Biologia e Patologia Molecolari CNR, Dipartimento di Scienze Biochimiche, Università La Sapienza, P.le A. Moro, 5, 00185 Roma, Italy

Received December 30, 2004; Revised Manuscript Received February 17, 2005

ABSTRACT: *Listeria innocua* Dps (*D*NA binding *p*rotein from *s*tarved cells) affords protection to DNA against oxidative damage and can accumulate about 500 iron atoms within its central cavity through a process facilitated by a ferroxidase center. The chemistry of iron binding and oxidation in *Listeria* Dps (*Li*Dps, formerly described as a ferritin) using H_2O_2 as oxidant was studied to further define the mechanism of iron deposition inside the protein and the role of *Li*Dps in protecting DNA from oxidative damage. The relatively strong binding of 12 Fe^{2+} to the apoprotein ($K_D \sim 0.023\ \mu M$) was demonstrated by isothermal titration calorimetry, fluorescence quenching, and pH stat experiments. Hydrogen peroxide was found to be a more efficient oxidant for the protein-bound Fe^{2+} than O_2. Iron(II) oxidation by H_2O_2 occurs with a stoichiometry of 2 Fe^{2+}/H_2O_2 in both the protein-based ferroxidation and subsequent mineralization reactions, indicating complete reduction of H_2O_2 to H_2O. Electron paramagnetic resonance (EPR) spin-trapping experiments demonstrated that *Li*Dps attenuates the production of hydroxyl radical by Fenton chemistry. DNA cleavage assays showed that the protein, while not binding to DNA itself, protects it against the deleterious combination of Fe^{2+} and H_2O_2. The overall process of iron deposition and detoxification by *Li*Dps is described by the following equations. For ferroxidation, $Fe^{2+} + Dps^{Z} \rightarrow [(Fe^{2+})\text{-}Dps]^{Z+1} + H^+$ (Fe^{2+} binding) and $[(Fe^{2+})\text{-}Dps]^{Z+1} + Fe^{2+} + H_2O_2 \rightarrow [(Fe^{3+})_2(O)_2\text{-}Dps]^{Z+1} + 2H^+$ (Fe^{2+} oxidation/hydrolysis). For mineralization, $2Fe^{2+} + H_2O_2 + 2H_2O \rightarrow 2Fe(O)OH_{(core)} + 4H^+$ (Fe^{2+} oxidation/hydrolysis). These reactions occur in place of undesirable odd-electron redox processes that produce hydroxyl radical.

The Dps protein (*D*NA-binding *p*rotein from *s*tarved cells) from the Gram-positive bacterium *Listeria innocua* can accumulate iron atoms within its central cavity to produce a hydrous ferric oxide mineral core (*1*−*4*) similar to that of typical ferritins (*5*−*8*). *Listeria* Dps, *Li*Dps[1] (previously known as *Listeria* ferritin), sequesters iron in three different reaction phases: iron binding to the ferroxidase centers, oxidation by dissolved oxygen, and mineralization to form a microcrystalline structure (*2*, *4*). An in vitro study has revealed that the 12 putative iron binding ferroxidase centers of *Li*Dps are important in iron binding and its rapid oxidation (*9*), similar to the canonical ferritins (*10*−*15*).

Despite this resemblance, the amino acid sequence of *Li*Dps shows no correspondence with that of a typical ferritin but rather exhibits significant similarity with the sequence of the Dps family members (*1*, *3*, *16*, *17*) and is most appropriately called a Dps protein. Dps proteins are widely distributed in a variety of bacteria, protecting DNA against the damage from the toxic oxygen compounds such as $O_2^{\bullet}$, H_2O_2, or $^{\bullet}OH$, a property correlated to their ferritin-like functions (*18*−*26*).

Crystallographic studies reveal that *Li*Dps is a dodecamer with 3/2 tetrahedral symmetry (*9*), a common architecture of the Dps family of proteins (*18*−*23*) and contrasting with the typical ferritins composed of 24 subunits arranged in 4/3/2 octahedral symmetry (*6*−*8*). The hollow shell of *Li*Dps has an internal diameter of about 40 Å, approximately half that found in ferritins, explaining its ability to sequester much less iron (∼500 Fe/shell) than the ferritins (∼4500 Fe/shell).

Like most other members of the Dps family, *Li*Dps is formed from a single type of 18 kDa subunit, in contrast to the two types of subunits, H and L, of mammalian ferritins. The secondary structure of *Li*Dps shows that each subunit is folded into a four-helical bundle (A−D) similar to that of the typical ferritins but without the C-terminal E helix (*9*). Two conserved iron-binding sites make up each of the 12 diiron ferroxidase centers which are located at the interface

† This work was supported by NIH Grant R01 GM 20194 (N.D.C.) and Grants PRIN 2002 (S.S.) and Fondazione Pasteur Cenci-Bolognetti and MIUR FIRB 2001 (E.C.).

* To whom correspondence should be addressed. Phone: (603) 862-2520. Fax: (603) 862-4278. E-mail: ndc@cisunix.unh.edu.

‡ University of New Hampshire.

§ Università La Sapienza.

[1] Abbreviations: EMPO, 5-ethoxycarbonyl-5-methyl-1-pyrroline *N*-oxide; EPR, electron paramagnetic resonance; ITC, isothermal titration calorimetry; *Li*Dps, *Listeria innocua* Dps; Mops, 3-(*N*-morpholino)-propanesulfonic acid.

10.1021/bi0472705 CCC: $30.25
Published on Web 03/23/2005

of two symmetry-related subunits instead of within the four-helix bundle of the H-chain as in mammalian ferritins (*8*). The amino acid residues constituting the ferroxidase centers of Dps proteins and ferritins differ as well (*8*, *9*).

An earlier study of *Li*Dps suggested that H_2O_2 is a superior oxidant for Fe^{2+} than O_2, but the phenomenon was not investigated in detail (*4*). More recent work has shown that, in the case of *Escherichia coli* Dps, the protein specifically facilitates the reaction of H_2O_2 with Fe^{2+} in a pairwise fashion such that Fenton chemistry is avoided, accounting in part for the protective effect of the protein against oxidative damage of DNA (*24*). In light of the fact that the *L. innocua* protein is now recognized to belong to the Dps family, we have undertaken a more detailed study of its iron oxidation and DNA protection properties. In the present work, the chemistry of Fe^{2+} binding and oxidation and Fe^{3+} hydrolysis were studied by UV−visible spectrophotometry, fluorescence, electrode oximetry, pH stat, and electron paramagnetic resonance (EPR) spin-trapping experiments. The stoichiometry of Fe^{2+} binding to the apoprotein has been defined and the reaction chemistry between Fe^{2+} and H_2O_2 established. In vitro DNA protection assays show that the protein protects DNA from oxidative damage through Fenton chemistry. The results demonstrate that *Li*Dps exhibits structure−function relationships characteristic of a Dps protein while sharing some features with the ferritins.

MATERIALS AND METHODS

The recombinant wild type was prepared as described elsewhere (*27*). The iron-free protein (apoprotein) was prepared according to the procedures previously described (*28*). The concentration of apoprotein was determined spectrophotometrically using a molar absorptivity of 2.59×10^{-5} M^{-1} cm^{-1} at 280 nm on a 12-mer protein basis (*4*). Trace iron in the apoprotein was determined by the ferrozine method following published procedures (*29*) and found to be typically ≤ 1.5 Fe/12-mer protein. Freshly prepared hydrogen peroxide solution was assayed by its absorbance at 240 nm ($\epsilon = 43.6$ M^{-1} cm^{-1}) or by measuring the concentration of O_2 produced upon addition of beef liver catalase (65000 units/mg; Boehringer Mannheim GmbH, Germany) to the H_2O_2 solution using Clark electrode oximetry (*30*). Hydrogen peroxide was purchased from Walgreen Co. (Deerfield, IL), ferrous sulfate from Baker Scientific Inc. of VWR Scientific (Plainfield, NJ), the Amplex Red hydrogen peroxide assay kit from Molecular Probes (Eugene, OR), and 5-ethoxycarbonyl-5-methyl-1-pyrroline *N*-oxide (EMPO) from Oxis Research (Portland, OR). All other chemicals were of reagent grade or better.

For anaerobic experiments, all solutions including water and buffer were thoroughly deoxygenated using high purity grade argon gas (99.995%, <5 ppm O_2). Syringes and 1 mL quartz cuvettes for absorbance or fluorescence measurements were O_2 purged with pure argon before filling with the deoxygenated solutions. A constant pressure of pure argon was maintained through a rubber septum on the cuvette during the experiment to prevent the diffusion of oxygen into the reaction solution.

UV−visible difference spectrophotometric titration and the kinetics of Fe^{2+} oxidation by H_2O_2 in *Li*Dps were performed on a Varian Cary 50 spectrophotometer at 25 °C with the reaction mixture constantly stirred using a micro stir bar in the bottom of the cuvette. Absorbance kinetic traces were collected using the Cary 50 kinetic software. The kinetic data were further analyzed with Origin 7.0 software (Microcal Inc.). The early portion of the absorbance $Y(t)$ vs time kinetic curve for Fe^{2+} oxidation by O_2 or H_2O_2 was fit to a third-order polynomial, $Y(t) = a_0 + a_1t + a_2t^2 + a_3t^3$, yielding the initial rate a_1.

X-band EPR spectra were measured at room temperature on a Bruker EleXsys E500 spectrometer fitted with a high-sensitivity SHQ cavity. A 2.0 mm i.d. quartz tube holding a 1.0 mm i.d. capillary containing 40 μL of sample solution was employed. The instrumental conditions were as follows: microwave power, 5.14 mW (16 dB attenuation); microwave frequency, 9.86 GHz; modulation frequency, 100 kHz; modulation amplitude, 1.0 G; receiver gain, 70 dB; time constant, 163.84 ms; sweep time, 83.89 s; scan number, 4; sweep width, 70 G; center field, 3507 G. In the EMPO spin-trapping experiments for hydroxyl radical (*31*), all spectra were recorded exactly 6 min after the last injection of H_2O_2. The conditions of the experiment are indicated in the figure legends.

Fluorescence measurements were carried out on a Varian Cary Eclipse fluorometer. Anaerobic titrations of Fe^{3+} binding were performed in a 1 cm path-length gastight quartz cell under an argon atmosphere with incremental additions of 4 Fe^{2+}/protein followed by 0.5 H_2O_2/Fe^{2+}. The production of H_2O_2 from iron oxidation by molecular oxygen in *Li*Dps was detected by Amplex Red−horseradish peroxidase (HRP) assay in 50 mM 3-(*N*-morpholino)propanesulfonic acid (Mops) buffer, pH = 7.4 (*30*). Fluorescence standards for the assay were plotted using duplicate samples and measured at the same time as the unknown samples, which were both incubated for 30 min at room temperature and protected from light.

The production of H^+ ion during Fe^{2+} binding and oxidation and Fe^{3+} hydrolysis was made with a pH stat/oximetry apparatus described elsewhere (*12*, *13*). O_2 consumption upon Fe^{2+} oxidation and O_2 evolution after injection of catalase were monitored by a Clark oxygen microelectrode. As a control, freshly prepared ferrous sulfate solution at pH 2.8 was added to a weakly buffered solution (0.3 mM Mops and 100 mM NaCl, pH stat 7.0). Background corrections for the free acid in the ferrous sulfate solutions (0.21 H^+/Fe^{2+}) were made in all calculations.

Isothermal titration calorimetry (ITC) of Fe^{2+} binding to apo-*Li*Dps was carried out at 25 °C with an upgraded Calorimetry Sciences Corp. CSC Model 4200 isothermal titration calorimeter as described for similar experiments with human H-chain ferritin (*14*).

DNA protection assays were conducted following the protocol for *Agrobacterium tumefaciens* Dps (*23*). Briefly, 30 nM pET-11a plasmid DNA in 30 mM Tris-HCl and 0.2 M NaCl, pH 7.3, buffer was allowed to interact with 3 μM *L. innocua* Dps or *E. coli* Dps for 10 min at room temperature and thereafter was subjected to 10 mM H_2O_2 or a combination of 10 mM H_2O_2 and 144 μM Fe(II). The reaction was stopped after 3 min by treatment with 2% SDS at 85 °C. The integrity of the DNA following the various treatments was assayed by 1% agarose gel electrophoresis.

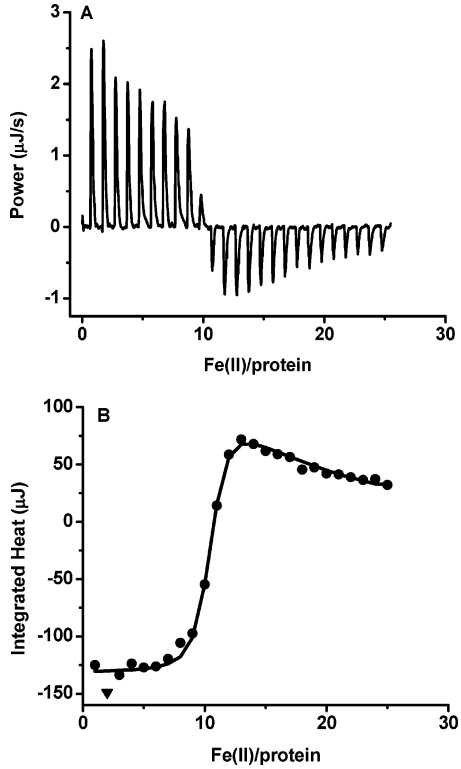

FIGURE 1: Isothermal titration calorimetric measurement of Fe^{2+} binding to *Li*Dps under anaerobic conditions. (A) Raw data. (B) Integrated heats. Conditions are as follows: 8.0 μM *Li*Dps, [dithionite] = 1 mM, stock [Fe^{2+}] = 1.0 mM, each point represents 1 Fe^{2+}/protein, 0.1 M Mops, pH = 7.0. Injections of Fe(II) were made every 5 min.

RESULTS

Fe^{2+} Binding to Listeria Dps. The binding stoichiometry of Fe(II) with apo-*Li*Dps was established by a combination of isothermal titration calorimetry (ITC), fluorescence spectrophotometric titration, and proton production measurements. Figure 1A shows the raw ITC data for the anaerobic titration of the protein with Fe^{2+} in 1 Fe^{2+}/protein increments. The integrated heats for each addition shown in Figure 1B were satisfactorily fit to a model of two independent classes of binding sites (strong and weak), yielding binding parameters for the strong sites of $n_1 = 10.9 \pm 0.3$, $K_1 = (4.4 \pm 1.7) \times 10^7\ M^{-1}$, $\Delta H_1^\circ = -12.9 \pm 0.4$ kJ/mol, $\Delta G_1^\circ = -37.9 \pm 0.4$ kJ/mol, and $\Delta S_1^\circ = 83.7 \pm 0.5$ J/(K·mol). For the weak sites, only the product of binding parameters $n_2 \cdot K_2 \cdot \Delta H_2^\circ = (2.0 \pm 1.1) \times 10^6\ M^{-1}$·kJ/mol could be determined since the individual parameters were correlated to one another as is typical of weak binding phenomena where the fitting is relatively insensitive to the values of the individual parameters in the concentration regime employed in the titration (see footnote 3 of ref *14*).

The ITC data indicate that there are $n_1 \sim 10-12$ strong binding sites on the protein. This stoichiometry was confirmed by an anaerobic Fe^{2+} titration of the apoprotein while monitoring the quenching of tryptophan fluorescence. As shown in Figure 2, fluorescence reaches a minimum once ~12 Fe^{2+} have been added to the protein.

Figure 3A shows the production of H^+ ion upon the anaerobic addition of two increments of 12 Fe^{2+} to the apoprotein as measured with the pH stat apparatus. After correction for the H^+ in the Fe^{2+} solution (0.21 H^+/Fe^{2+}), we calculate that 1.0 H^+ is generated per Fe^{2+} for addition of the first 12 Fe^{2+}, dropping to only 0.17 H^+/Fe^{2+} for the second addition of 12 Fe^{2+}. This result is in accord with a binding stoichiometry of 12 Fe^{2+}/protein for the strong sites followed by a much weaker interaction beyond the first 12 Fe^{2+}added. Therefore, we write the equation for Fe^{2+} binding to each of the 12 strong sites of *Li*Dps as

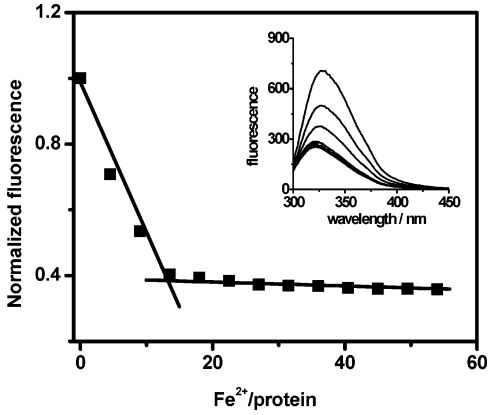

FIGURE 2: Fluorescence quenching upon Fe^{2+} anaerobically binding to *Li*Dps. Conditions are as follows: $\lambda_{ex} = 280$ nm, $\lambda_{em} = 335$ nm, slits for both excitation and emission are 5 nm, 2.0 μM *Li*Dps, 0.1 M Mops, 0.05 M NaCl, pH = 7.0, 25 °C.

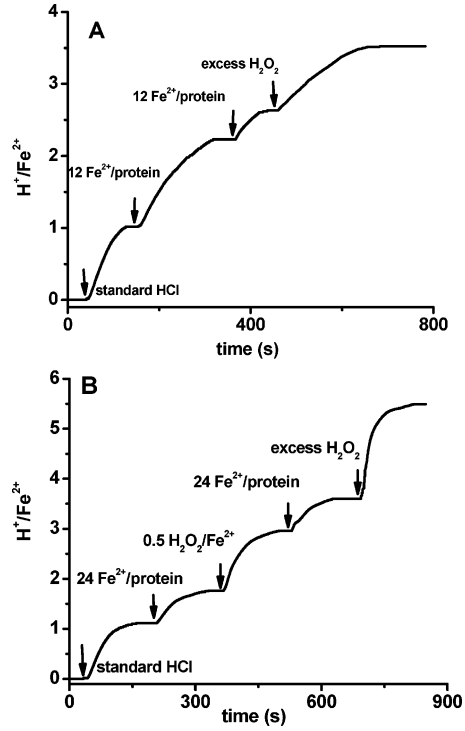

FIGURE 3: Proton production upon Fe^{2+} oxidation in the protein-based ferroxidation (A) and mineralization reactions (B). Conditions are as follows: anaerobic, 5.0 μM protein, 0.3 mM Mops, 0.1 M NaCl, pH stat 7.0, 5 mM standard NaOH, 25 μM standard HCl.

$$Fe^{2+} + Dps^Z \rightarrow [(Fe^{2+})\text{-}Dps]^{Z+1} + H^+ \qquad (1)$$

Kinetics of Fe^{2+} Oxidation by O_2 versus H_2O_2. Consumption of dissolved molecular oxygen (~280 μM) during iron oxidation in the presence and absence of apo-*Li*Dps was measured by electrode oximetry. Oxidation of Fe^{2+} by O_2 in the presence of *Li*Dps was found to be very slow (Figure 4, curve a), being comparable to that of autoxidation in buffer

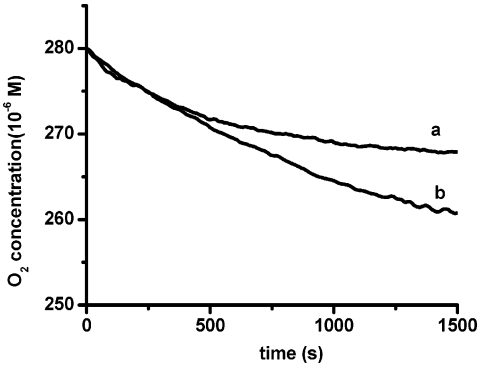

FIGURE 4: O_2 consumption curves in *Li*Dps (curve a) and in the buffer (curve b) upon addition of Fe^{2+} to the solution. Conditions are as follows: 280 μM O_2, 90 μM Fe^{2+}, 0.05 M Mops and NaCl, pH stat 7.0, 25 °C. (a) In 4.5 μM *Li*Dps. (b) In buffer.

alone for the first 500 s of the reaction but ultimately slowing further (Figure 4, cf. curves a and b). In the experiment depicted in Figure 4 (curve a), the aerobic addition of 90 μM Fe^{2+} (20 Fe^{2+}/protein) resulted in the consumption of only 7.6 μM O_2 during the 1500 s of the reaction, implying that some of the Fe^{2+} remained unoxidized at this point in time. The Fe^{2+} remaining in solution was determined to be 57.1 μM by the ferrozine assay. From the 7.6 μM O_2 consumed and the amount of Fe^{2+} oxidized (90.0 − 57.1 = 32.9 μM), a stoichiometry of 4.3 Fe^{2+}/O_2 was calculated, in agreement with the previously reported iron oxidation stoichiometry by dioxygen of ∼4 Fe^{2+}/O_2 (*4*).

H_2O_2 has been shown to be a more efficient oxidant for Fe^{2+} in *E. coli* Dps than O_2 (*24*) and also suggested to be a better oxidant in *Li*Dps (*4*). Therefore, a direct comparison of the rates of iron oxidation in *Li*Dps by H_2O_2 versus by O_2 was undertaken. Iron oxidation in *Li*Dps was monitored at λ = 304 nm (the maximum absorbance of Fe^{3+}−protein complex) and 25 °C after the addition of 24 Fe^{2+}/protein to the apoprotein solution containing either H_2O_2 (Figure 5, curve a) or O_2 (curve b). The initial rate of Fe^{2+} oxidation by H_2O_2 is ∼1000-fold faster [υ_0 = 16.7 ± 1.7 mol of Fe (mol of protein)$^{-1}$ s^{-1}] than by O_2 [υ_0 = 0.0160 ± 0.0003 mol of Fe (mol of protein)$^{-1}$ s^{-1}], indicating that H_2O_2 is a far superior oxidant.

H_2O_2 Production during Fe^{2+} Oxidation by O_2. The fluorescence assay of H_2O_2 using Amplex Red was performed to determine whether H_2O_2 is an intermediate product during Fe^{2+} oxidation by O_2 in both ferroxidation and mineralization reactions. Hydrogen peroxide generated in this way would be expected to rapidly react with additional Fe^{2+} in the solution. In the Amplex Red assay, an average of one H_2O_2 was detected per 5.7 Fe^{2+}oxidized for the ferroxidation reaction for the aerobic addition sequence: Amplex Red + HRP + apo-*Li*Dps + 24 Fe^{2+}/protein. For the mineralization reaction, one H_2O_2 was observed per 14.9 Fe^{2+} oxidized for the sequence: Amplex Red + HRP + apo-*Li*Dps + 100 Fe^{2+}/protein. The control experiment of Amplex Red + HRP + 7.2 μM Fe^{2+} showed only a very weak fluorescence signal at the detection wavelength of 585 nm. We conclude that, in both the ferroxidation and mineralization reactions, H_2O_2 is an intermediate product of Fe^{2+} oxidation by O_2. The H_2O_2 thus produced presumably reacts rapidly with further Fe^{2+} to give the observed net Fe^{2+}/O_2 stoichiometry of 4/1, accounting for the complete reduction of O_2 to H_2O.

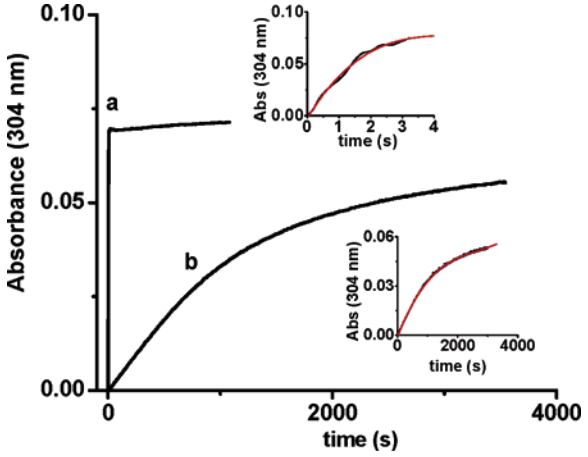

FIGURE 5: Kinetics of Fe^{2+} oxidation by H_2O_2 (curve a) and O_2 (curve b) in *Li*Dps. The upper and lower insets show the early portions of curves a and b and the corresponding cubic equation fits giving the values for the parameters a_0, a_1, a_2, and a_3 of −0.00235, 0.0504, −0.0107, and 7.718 × 10^{-4} and of −0.000862, 4.70 × 10^{-5}, −1.53 × 10^{-8}, and 1.904 × 10^{-12}, respectively (see Materials and Methods). The initial rates were derived from the linear a_1 coefficients 0.0504 and 4.70 × 10^{-5} for H_2O_2 and O_2, respectively. Conditions are as follows: 0.1 M Mops, 0.05 M NaCl, pH 7.0, 25 °C. (a) *Li*Dps + 24 Fe^{2+}/protein + H_2O_2 , anaerobic, 1.17 μM *Li*Dps, 28.1 μM Fe^{2+}, 100 μM H_2O_2. (b) *Li*Dps + O_2 + 24 Fe^{2+}/protein, aerobic, 1.18 μM *Li*Dps, 28.3 μM Fe^{2+}, 280 μM O_2.

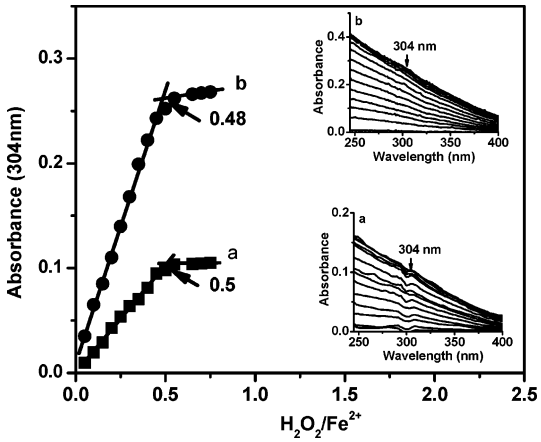

FIGURE 6: H_2O_2 titration curves for Fe^{2+} oxidation in *Li*Dps with the different loading of iron. Each point corresponds to an addition of 0.05 H_2O_2/Fe^{2+}. Conditions: anaerobic, 0.1 M Mops, 0.05 M NaCl, pH 7.0. (a) 1.8 μM *Li*Dps + 43.2 μM Fe^{2+} (24 Fe^{2+}/protein). (b) 1.1 μM *Li*Dps + 110 μM Fe^{2+}(100 Fe^{2+}/protein). Inset: Family of UV−visible difference spectra for ferroxidation (a) and mineralization (b) reactions.

Stoichiometry of Fe^{2+} Oxidation by H_2O_2. Anaerobic addition of Fe^{2+} to *Li*Dps (24 Fe^{2+}/protein) showed no UV absorbance, whereas a band with a maximum absorbance at 304 nm emerged upon subsequent addition of H_2O_2 (Figure 6, inset a). The molar absorptivity for this oxidation production was determined to be ϵ_{304nm} = 2550 M^{-1} cm^{-1} per iron and is within the range of values for dinuclear Fe^{3+} complexes formed at the ferroxidase site of ferritins (∼3000 M^{-1} cm^{-1} per iron) (*12*, *13*, *24*, *30*). Therefore, the absorbing compound is postulated to be a μ-oxo-bridged dinuclear Fe^{3+}−protein complex. To establish the stoichiometry of oxidation, an anaerobic titration of protein solutions containing either 24 Fe^{2+}/protein (ferroxidation) or 100 Fe^{2+}/protein (mineralization) with increments of 0.05 H_2O_2/Fe^{2+} was

carried out. Stoichiometries of ~0.5 H_2O_2/Fe^{2+} were obtained as shown in Figure 6, curves a and b, respectively, indicating complete reduction of H_2O_2 to H_2O in both instances; i.e., two Fe^{2+} are oxidized per H_2O_2 consumed.

A stoichiometry of 0.5 H_2O_2/Fe^{2+} for the ferroxidation reaction was also obtained using electrode oximetry performed under anaerobic conditions. In this experiment, excess H_2O_2 was added to the *Li*Dps solution containing 24 Fe^{2+}/protein followed by injection of 1 μL of catalase (50 s after injection of H_2O_2). From the amount of O_2 produced from the unreacted H_2O_2 [$H_2O_2 \rightarrow H_2O + {}^1/_2O_2$ (*14*)], the amount of H_2O_2 that had been consumed by Fe^{2+} was calculated. For the addition sequence 2 μM apo-*Li*Dps + 48 μM Fe^{2+} + 100 μM H_2O_2 + catalase, 37 μM O_2 was produced, indicating that 74 μM unreacted H_2O_2 was present; therefore, 26 μM H_2O_2 had reacted with the 48 μM Fe^{2+} to give a stoichiometry of ~0.5 H_2O_2/Fe^{2+}. In a control experiment without *Li*Dps present for the addition sequence buffer + 48 μM Fe^{2+} + 100 μM H_2O_2 + catalase, 25 μM O_2 was produced, demonstrating that 50 μM H_2O_2 had reacted with 48 μM Fe^{2+} to give the stoichiometry of ~1 Fe^{2+}/H_2O_2, the value expected from the Fenton reaction ($Fe^{2+} + H_2O_2 \rightarrow Fe^{3+} + OH^- + {}^{\bullet}OH$). Thus, the mechanism of iron oxidation is altered by *Li*Dps, switching the oxidation stoichiometry from 0.5 H_2O_2/Fe^{2+} in its presence to 1 H_2O_2/Fe^{2+} in its absence, a result in accord with attenuation of Fenton chemistry by the protein. This result was verified by the EPR spin trapping experiments described below.

Stoichiometric Equations for Iron Oxidation and Hydrolysis. For the ferroxidase reaction, one H^+ is produced per Fe^{2+} oxidized by H_2O_2 when a total of 24 Fe^{2+} are added to the protein followed by H_2O_2 (Figure 3A), whereas for the mineralization reaction, 2 H^+ are produced per Fe^{2+} when a second 24 Fe^{2+} are added to the protein followed by H_2O_2 (Figure 3B). On the basis of the stoichiometries of Fe^{2+} binding, oxidation and proton production, and the fact that 24 Fe^{3+} have been shown to bind to the apoprotein when Fe^{2+} is oxidized by H_2O_2 (*32*), we write the stoichiometric equation for Fe^{2+} oxidation at each of the 12 ferroxidase centers as follows:

$$[(Fe^{2+})\text{-Dps}]^{Z+1} + Fe^{2+} + H_2O_2 \rightarrow [(Fe^{3+})_2(O)_2\text{-Dps}]^{Z+1} + 2H^+ \quad (2)$$

The oxidation/hydrolysis reaction for the mineralization phase of core formation is given by the equation:

$$2Fe^{2+} + H_2O_2 + 2H_2O \rightarrow 2Fe(O)OH_{(core)} + 4H^+ \quad (3)$$

Attenuation of Hydroxyl Radical Production. The ability of *Li*Dps to minimize the production of hydroxyl radical arising from the Fenton reaction was investigated by spin-trapping experiments (Figure 7). Spectrum a is that of the EMPO−OH adduct for the control experiment in the absence of protein: EMPO + Fe^{2+} + H_2O_2. The oxidation of Fe^{2+} by H_2O_2 generates hydroxyl radical, and thus an intense spectrum from trapped $HO^{\bullet}$ was observed. Spectrum b is that for another control experiment for the addition sequence: bovine serum albumin (BSA) + EMPO + Fe^{2+} + H_2O_2. Again, an intense spectrum was obtained. In contrast, for the addition sequence apo-*Li*Dps + EMPO + 24 or 100 $Fe^{2+}/$*Li*Dps + H_2O_2, weak EPR signals were obtained

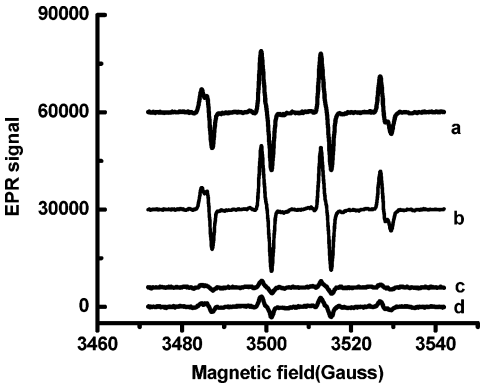

FIGURE 7: X-band EPR signal of the EMPO−OH adduct: spectrum a, anaerobic addition sequence EMPO + Fe^{2+} + H_2O_2; spectrum b, BSA + EMPO + Fe^{2+} + H_2O_2; spectrum c, *Li*Dps + EMPO + 24 Fe^{2+}/protein + H_2O_2; spectrum d, *Li*Dps + EMPO + 100 Fe^{2+}/protein + H_2O_2. Conditions: 5.0 μM proteins, 37.5 mM EMPO, 120 μM Fe^{2+} (spectra a−c) or 500 μM Fe^{2+} (spectrum d), 150 μM H_2O_2 (spectra a−c) or 500 μM H_2O_2 (spectrum d) added in 10 increments of either 15 μM H_2O_2 or 50 μM H_2O_2.

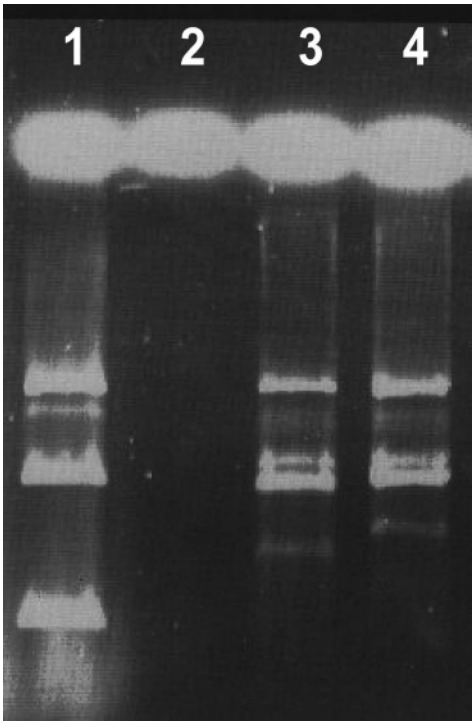

FIGURE 8: DNA protection assay. Agarose gel electrophoresis. Lanes: 1, DNA + H_2O_2; 2, DNA + H_2O_2 + Fe(II); 3, DNA + *L. innocua* Dps + H_2O_2 + Fe(II); 4, DNA + *E. coli* Dps + H_2O_2 + Fe(II). Conditions: 30 nM plasmid DNA in 30 mM Tris-HCl, 0.2 M NaCl, pH 7.3, buffer subjected to 10 mM H_2O_2 or a combination of 10 mM H_2O_2 and 144 μM Fe(II) in the presence or absence of 3 μM Dps. Bands from top to bottom correspond to increasing degrees of supercoiling of the DNA.

(spectra c and d), demonstrating that *Li*Dps attenuates hydroxyl radical production, a result in accord with the measured 2 Fe^{2+}/H_2O_2 oxidation stoichiometry of eqs 2 and 3 (Figure 6).

DNA Protection by LiDps. Figure 8 illustrates the results of DNA protection/degradation experiments. Treatment with H_2O_2 alone has no effect on the gel pattern of plasmid DNA (compare lane 1 with Figure 6 of ref *23*) whereas treatment with H_2O_2 + Fe(II) fully degrades the DNA (lane 2). In

contrast, the presence of either *L. innocua* Dps (lane 3) or *E. coli* Dps (lane 4) DNA is essentially undegraded.

DISCUSSION

*Li*Dps is a representative system for the study of iron accumulation within the structurally unique proteins of the Dps ferritin-like family. The present work reveals that *Li*Dps has some characteristics similar to *E. coli* Dps but exhibits differences as well. In both proteins, H_2O_2 is a more efficient oxidant for Fe^{2+} than molecular oxygen (Figure 5), which contrasts with the typical ferritins where O_2 is an efficient oxidant for Fe^{2+} bound at specific sites of the protein (*8*, *12*, *13*). In *Li*Dps, the oxidation of Fe^{2+} in both ferroxidation and mineralization reactions proceeds rapidly and completely with the stoichiometry of 2 Fe^{2+}/H_2O_2 (Figure 6), thus preventing the formation of the significant amounts of hydroxyl radical from the Fenton chemistry, a finding confirmed by EPR spin-trapping experiments (Figure 7). Similar behavior is seen with *E. coli* Dps (*24*), and both proteins protect DNA (Figure 8). The similarity in the iron chemistries of *Li*Dps and *E. coli* Dps is in keeping with the conservation of the ferroxidase center ligands for the two proteins (*17*). All Dps proteins have sequence similarity and a common overall architecture (*16*−*21*, *33*, *34*), suggesting that all may share some common features in iron accumulation.

Fe^{2+} oxidation by O_2 in Dps proteins is markedly slower than in mammalian and bacterial ferritins (*12*, *13*, *24*) and is comparable to that in buffer in the absence of Dps protein (Figure 4). Dps is better suited to utilize H_2O_2 as the oxidant (Figure 5) whereas mammalian ferritins utilize O_2, implying different preferred substrates for iron oxidation in vivo for the two classes of proteins. The faster initial rates of Fe^{2+} oxidization by H_2O_2 during the ferroxidation reaction of *Li*Dps than during the mineralization reaction (*32*) are opposite to the observations made with O_2 as oxidant where the ferroxidation reaction proceeded more slowly than the oxidation/mineralization reaction (*4*), a further indication that H_2O_2 is the preferred oxidant in the ferroxidase reaction. The production of 2 H^+ upon the oxidation of the di-Fe^{2+} center in *Li*Dps (reaction 2) is the same as that observed previously using O_2 as oxidant (*4*), suggesting similar Fe^{3+} hydrolysis products in both instances. Both oxidants are capable of oxidizing Fe^{2+} to generate $Fe(O)OH_{(s)}$ cores.

The different iron oxidation properties of the ferritins and Dps proteins are reflected in their different ferroxidase centers. Tyrosine-34 near the ferroxidase center of H-chain ferritins may be important in rapid ferroxidation (*35*, *36*), but this residue is absent in Dps proteins. Perhaps more importantly is that the ferroxidase center of *Li*Dps has two histidine residues, His31 and His43, one located at each Fe binding site (*9*), whereas vertebrate ferritins have only one His residue (*8*). Like *Li*Dps, both *E. coli* bacterioferritin and *E. coli* Dps have two histidine residues at their ferroxidase centers. These proteins prefer H_2O_2 over O_2 as the Fe(II) oxidant, exhibit iron oxidation stoichiometries of 2 Fe(II)/H_2O_2 and 4 Fe(II)/O_2, and do not turn over iron at their centers or do so slowly (*13*, *24*, *30*). These properties are shared in common with *Li*Dps. In addition, *E. coli* bacterioferritin also inhibits Fenton chemistry (*30*). Thus the presence of two histidine residues in the ferroxidase center seems to alter the catalytic properties of the protein in significant ways so as to favor H_2O_2 over O_2 as the oxidant, leading to the attenuation of Fenton chemistry.

The ITC, fluorescence quenching, and pH stat data show that ∼12 Fe^{2+} bind to apo-*Li*Dps with relatively strong affinity ($K_D = 0.023\ \mu M$). This result differs from the binding stoichiometry of 24 Fe^{2+} seen with *E. coli* Dps (*24*), despite conservation of ferroxidase center residues, and with the 24 Fe^{2+}/protein binding stoichiometry previously assumed for *Li*Dps (*4*). In contrast to *E. coli* Dps where 2 Fe^{2+} bind to the ferroxidase center prior to oxidation by H_2O_2 (*24*), in *Li*Dps, a second Fe^{2+} binds and oxidizes at each of the 12 ferroxidase centers only upon addition of H_2O_2 as in eq 2. Obviously, structural factors beyond the identity of the ferroxidase center ligands play a role in binding, e.g., charged residues in the vicinity of the ferroxidase center, like Lys48 in *E. coli* Dps where it can serve as a further metal ligand in the binding of Pb (*18*).

Fe^{2+} binding in *Li*Dps is favored both enthalpically ($\Delta H^\circ = -12.9$ kJ/mol) and entropically [$\Delta S^\circ = 83.7$ J/(K·mol)] with the entropy being the dominant term ($-T\Delta S^\circ = -24.9$ kJ/mol) in the standard free energy of binding ($\Delta G^\circ = \Delta H^\circ - T\Delta S^\circ$). Binding of Fe^{2+}, Zn^{2+}, and Tb^{3+} to human H-chain ferritin (*14*, *37*) and Fe^{2+} to *E. coli* frataxin (*38*) is also largely driven by entropy. The large positive entropy changes are likely a consequence of changes in metal ion hydration upon complexation of the metal ion with the protein, releasing water from the first coordination sphere of Fe^{2+} (*37*). Although the association constant for Fe^{2+} binding to *E. coli* Dps has not been measured, binding must be reasonably strong and comparable to that of *Li*Dps since sharp end points are obtained in titration of the apoprotein with Fe^{2+} (*24*). Fe^{2+} binding to human H-chain ferritin ($K_D \sim 7\ \mu M$) and *E. coli* and human frataxins ($K_D \sim 4$ and 55 μM, respectively) (*38*, *39*) is ∼200−2500-fold weaker than seen in *Li*Dps ($K_D \sim 0.02\ \mu M$). Thus *Li*Dps has avidity for Fe^{2+} that significantly exceeds that of other known iron-binding proteins for which Fe^{2+} binding affinities have been measured.

In conclusion, the overall mechanism of iron deposition in the *Li*Dps using H_2O_2 as oxidant has been investigated and the detailed chemistry of iron binding and oxidation established. The pairwise oxidation of Fe^{2+} by H_2O_2 prevents the production of toxic hydroxyl radical, a property characteristic of the Dps family of proteins that is likely central to their role in protecting cells against oxidative stress. The in vitro assays demonstrate significant protection of DNA by *Li*Dps against Fenton chemistry.

REFERENCES

1. Ilari, A., Savino, C., Stefanini, S., Chiancone, E., and Tsernoglou, D. (1999) Crystallization and preliminary X-ray crystallographic analysis of the unusual ferritin from *Listeria innocua*, *Acta Crystallogr. D55*, 552−553.
2. Stefanini, S., Cavallo, S., Montagnini, B., and Chiancone, E. (1999) Incorporation of iron by the unusual dodecameric ferritin from *Listeria innocua*, *Biochem. J. 338*, 71−75.
3. Bozzi, M., Mignogna, G., Stefanini, S., Barra, D., Longhi, C., Valenti, P., and Chiancone, E. (1997) A novel non-heme iron-binding ferritin related to the DNA-binding proteins of the Dps family in *Listeria innocua*, *J. Biol. Chem. 272*, 3259−3265.
4. Yang, X., Chiancone, E., Stefanini, S., Ilari, A., and Chasteen, N. D. (2000) Iron oxidation and hydrolysis reactions of a novel ferritin from *Listeria innocua*, *Biochem. J. 349*, 783−786.

5. Andrews, S. C., Arosio, P., Bottke, W., Briat, J., von Darl, M., Harrison, P. M., Laulhère, J., Levi, S., Lobreaux, S., and Yewdall, S. J. (1992) Structure, function, and evolution of ferritin, *J. Inorg. Biochem. 47*, 161−174.
6. Proulx-Curry, P. M., and Chasteen, N. D. (1995) Molecular aspects of iron uptake and storage in ferritin, *Coord. Chem. Rev. 144*, 347−368.
7. Harrison, P. M., Hempstead, P. D., Artymiuk, P. J., and Andrews, S. C. (1998) *in Metal ions in biological systems* (Sigel, A., and Sigel, H., Eds.) Vol. 35, pp 435−477, Dekker, New York.
8. Chasteen, N. D., and Harrison, P. M. (1999) Mineralization in ferritin: an efficient means of iron storage, *J. Struct. Biol. 126*, 182−194.
9. Ilari, A., Stefanini, S., Chiancone, E., and Tsernoglou, D. (2000) The dodecameric ferritin from *Listeria innocua* contains a novel intersubunit iron-binding site, *Nat. Struct. Biol. 7*, 38−43.
10. Sun, S., Arosio, P., Levi, S., and Chasteen, N. D. (1993) Ferroxidase kinetics of human liver apoferritin, recombinant H-chain apoferritin, and site-directed mutants, *Biochemistry 32*, 9362−9369.
11. Sun, S., and Chasteen, N. D. (1992) Ferroxidase kinetics of horse spleen apoferritin, *J. Biol. Chem. 267*, 25160−25166.
12. Yang, X., Chen-Barrett, Y., Arosio, P., and Chasteen, N. D. (1998) Reaction paths of iron oxidation and hydrolysis in horse spleen and recombinant human ferritins, *Biochemistry 37*, 9743−9750.
13. Yang, X., Le Brun, N. E., Thomson, A. J., Moore, G. R., and Chasteen, N. D. (2000) The iron oxidation and hydrolysis chemistry of *Escherichia coli* bacterioferritin, *Biochemistry 39*, 4915−4923.
14. Bou-Abdallah, F., Arosio, P., Santambrogio, P., Yang, X., Janus-Chandler, C., and Chasteen, N. D. (2002) Ferrous ion binding to recombinant human H-chain ferritin. An isothermal titration calorimetry study, *Biochemistry 41*, 11184−11191.
15. Bou-Abdallah, F., Papaefthymiou, G. C., Scheswohl, D. M., Stanga, S. D., Arosio, P., and Chasteen, N. D. (2002) μ-1,2-Peroxobridged di-iron(III) dimer formation in human H-chain ferritin, *Biochem. J. 364*, 57−63.
16. Chiaraluce, R., Consalvi, V., Cavallo, S., Ilari, A., Stefanini, S., and Chiancone, E. (2000) The unusual dodecameric ferritin from *Listeria innocua* dissociates below pH 2.0, *Eur. J. Biochem. 267*, 5733−5741.
17. Ilari, A., Ceci, P., Ferrari, D., Rossi, G. L., and Chiancone, E. (2002) Iron incorporation into *Escherichia coli* Dps gives rise to a ferritin-like microcrystalline core, *J. Biol. Chem. 277*, 37619−37623.
18. Grant, R. A., Filman, D. J., Finkel, S. E., Kolter, R., and Hogle, J. M. (1998) The crystal structure of Dps, a ferritin homolog that binds and protects DNA, *Nat. Struct. Biol. 5*, 294−303.
19. Papinutto, E., Dundon, W. G., Pitulis, N., Battistutta, R., Montecucco, C., and Zanotti, G. (2002) Structure of two iron-binding proteins from *Bacillus anthracis*, *J. Biol. Chem. 277*, 15093−15098.
20. Kauko, A., Haataja, S., Pulliainen, A. T., Finne, J., and Papageorgiou, A. C. (2004) Crystal structure of *Streptococcus suis* Dps-like peroxide resistance protein Dpr: implications for iron incorporation, *J. Mol. Biol. 338*, 547−558.
21. Roy, S., Gupta, S., Das, S., Sekar, K., Chatterji, D., and Vijayan, M. (2004) X-ray analysis of *Mycobacterium smegmatis* Dps and a comparative study involving other Dps and Dps-like molecules, *J. Mol. Biol. 339*, 1103−1113.
22. Peña, M. M. O., and Bullerjahn, G. S. (1995) The DpsA protein of *Synechococcus* sp. strain PCC7942 is a DNA-binding hemoprotein, *J. Biol. Chem. 270*, 22478−22482.
23. Ceci, P., Ilari, A., Falvo, E., and Chiancone, E. (2003) The Dps protein of *Agrobacterium tumefaciens* does not bind to DNA but protects it toward oxidative cleavage, *J. Biol. Chem. 278*, 20319−20326.
24. Zhao, G., Ceci, P., Ilari, A., Giangiacomo, L., Laue, T. M., Chiancone, E., and Chasteen, N. D. (2002) Iron and hydrogen peroxide detoxification properties of DNA-binding protein from starved cells, *J. Biol. Chem. 277*, 27689−27696.
25. Yamamoto, Y., Poole, L. B., Hantgan, R. R., and Kamio, Y. (2002) An iron-binding protein, Dpr, from *Streptococcus mutans* prevents iron-dependent hydroxyl radical formation in vitro, *J. Bacteriol. 184*, 2931−2939.
26. Ishikawa, T., Mizunoe, Y., Kawabata, S., Takade, A., Harada, M., Wai, S. N., and Yoshida, S. (2003) The iron-binding protein Dps confers hydrogen peroxide stress resistance to *Campylobacter jejuni*, *J. Bacteriol. 185*, 1010−1017.
27. Polidoro, M., De Biase, D., Montagnini, B., Guarrera, L., Cavallo, S., Valenti, P., Stefanini, S., and Chiancone, E. (2002) The expression of the dodecameric ferritin in *Listeria* spp. is induced by iron limitation and stationary growth phase, *Gene 296*, 121−128.
28. Hanna, P. M., Chen, Y., and Chasteen, N. D. (1991) Initial iron oxidation in horse spleen apoferritin. Characterization of a mixed-valence iron(II)-iron(III) complex, *J. Biol. Chem. 266*, 886−893.
29. Percival, M. D. (1991) Human 5-lipoxygenase contains an essential iron, *J. Biol. Chem. 266*, 10058−10061.
30. Bou-Abdallah, F., Lewin, A. C., Le Brun, N. E., Moore, G. R., and Chasteen, N. D. (2002) Iron detoxification properties of *Escherichia coli* bacterioferritin, *J. Biol. Chem. 277*, 37064−37069.
31. Zhang, H., Joseph, J., Vasquez-Vivar, J., Karoui, H., Nsanzumuhire, C., Martásek, P., Tordo, P., and Kalyanaraman, B. (2000) Detection of superoxide anion using an isotopically labeled nitrone spin trap: potential biological applications, *FEBS Lett. 473*, 58−62.
32. Ilari, A., Latella, M. C., Ceci, P., Ribacchi, F., Su, M., Giangiacomo, L., Stefanini, S., Chasteen, N. D., and Chiancone, E. (2005) The unusual intersubunit ferroxidase center of *Listeria innocua* Dps is required for hydrogen peroxide detoxification but not for iron uptake. A study with site-specific mutants, *Biochemistry 44*, 5579−5587.
33. Ren, B., Tibbelin, G., Kajino, T., Asami, O., and Ladenstein, R. (2003) The multilayered structure of Dps with a novel di-nuclear ferroxidase center, *J. Mol. Biol. 329*, 467−477.
34. Zanotti, G., Papinutto, E., Dundon, W. G., Battistutta, R., Seveso, M., Giudice, G. D., Rappuoli, R., and Montecucco, C. (2002) Structure of the neutrophil-activating protein from *Helicobacter pylori*, *J. Mol. Biol. 323*, 125−130.
35. Treffry, A., Zhao, Z., Quail, M. A., Guest, J. R., and Harrison, P. M. (1995) Iron(II) oxidation by H chain ferritin: evidence from site-directed mutagenesis that a transient blue species is formed at the dinuclear iron center, *Biochemistry 34*, 15204−15213.
36. Fetter, J., Cohen, J., Danger, D., Sanders-Loehr, J., and Theil, E. C. (1997) The influence of conserved tyrosine 30 and tissue-dependent differences in sequence on ferritin function: use of blue and purple Fe(III) species as reporters of ferroxidation, *J. Biol. Inorg. Chem. 2*, 652−661.
37. Bou-Abdallah, F., Arosio, P., Levi, S., Janus-Chandler, C., and Chasteen, N. D. (2003) Defining metal ion inhibitor interactions with recombinant human H- and L-chain ferritins and site-directed variants: an isothermal titration calorimetry study, *J. Inorg. Biochem. 8*, 489−497.
38. Bou-Abdallah, F., Adinolfi, S., Pastore, A., Laue, T. M., and Chasteen, N. D. (2004) Iron binding and oxidation kinetics in frataxin CyaY of *Escherichia coli*, *J. Mol. Biol. 341*, 605−615.
39. Yoon, T., and Cowan, J. A. (2003) Iron-sulfur cluster biosynthesis. Characterization of frataxin as an iron donor for assembly of [2Fe-2S] clusters in ISU-type proteins, *J. Am. Chem. Soc. 125*, 6078−6084.

BI0472705